Available online at www.sciencedirect.com
SCIENCE DIRECT®
International Journal of Thermal Sciences 44 (2005) 540–546
International Journal of Thermal Sciences
www.elsevier.com/locate/ijts

On the thermal performance of an internally finned three-dimensional cubic enclosure in natural convection

A.K. da Silva [a,*], L. Gosselin [b]

[a] *Department of Mechanical Engineering and Materials Science, Duke University, Box 90300, Durham, NC 27708-300, USA*
[b] *Département de génie mécanique, Université Laval, Québec, Québec, G1K 7P4, Canada*

Received 15 January 2004; received in revised form 3 October 2004; accepted 10 November 2004

Abstract

The present paper evaluates the effect of the aspect ratio and horizontal length of a high conductivity rectangular fin attached to the hot wall of a three-dimensional differentially heated cubic enclosure in laminar natural convection. The objective is the augmentation of the heat transfer delivered from the heated wall to the fluid when the volume fraction of the fin is fixed. Two different values for the fin volume were considered: (i) a large fin that occupies 10 percent of the cubic enclosure, and (ii), a much smaller fin that occupies only 0.1 percent of the enclosure total volume. The finite element technique was applied for solving the coupled steady-state velocity and temperature fields in the 3-D domain in the range $10^3 < Ra < 10^5$, where Ra is the Rayleigh number based on the enclosure height. The numerical results showed that for an enclosure assisted by a large volume fraction fin, the fin aspect ratio does not play an important role, and the average heat flux transferred to the fluid increases monotonically with the fin horizontal length. For a cubic enclosure assisted by a small volume fraction fin, the average heat flux delivered to the fluid increases with the aspect ratio of the fin, and with the horizontal length of the fin. A scale analysis was used to predict the domain in which the fin geometry plays a significant role, i.e., when optimization opportunities are present.

Keywords: Electronic cooling; Natural convection; Cubic enclosure; Fin; Geometric optimization

1. Introduction

Due to its low cost and apparent simplicity, natural convection cooling (or heating) has always been an attractive technique in thermal engineering. The applications in which it is used are countless, embracing many technical fields. Examples are energy storage systems, thermal control of electronic devices and buildings. Such variety of applications has generated a large body of work that studied buoyancy driven flows in several configurations and different boundary conditions. One of the most examined configurations is the differentially heated cavity. Starting with Bénard [1], the behavior of such enclosured self-driven flows has been reported analytically, experimentally and numerically in several articles [2–7].

Nowadays, the demand for greater compactness is accompanied by a corresponding increase in volumetric and surface power dissipation. There is therefore a current call to pursue better configurations in order to maximize heat transfer rate. In spite of the constant pressure for more efficient heat transfer devices based on known techniques such as natural convection inside a cavity, very few papers deal with optimization of thermal performance [3,8,9]. Most of the bodywork found is of descriptive nature [10,11], in none of them heat transfer augmentation under global constraints was the main concern. This motivates the present study to further investigate theoretically and numerically the behavior of a class of improved enclosures.

The aim is to determine the ideal geometric features of a rectangular fin that maximizes the thermal performance of a differentially heated three-dimensional cubic enclosure

* Corresponding author. Tel.: +1 (919) 660-5299, fax: +1 (919) 660-8963.
E-mail address: akd3@duke.edu (A.K. da Silva).

1290-0729/$ – see front matter
doi:10.1016/j.ijthermalsci.2004.11.011

Nomenclature

a	fin width	m
A	area	m^2
b	fin length	m
c	fin height	m
c_P	specific heat	$J{\cdot}kg^{-1}{\cdot}K^{-1}$
g	gravity	$m{\cdot}s^{-2}$
H	cavity height	m
i	iteration index	
k	thermal conductivity	$W{\cdot}m^{-1}{\cdot}K^{-1}$
L	cavity length	m
n	normal vector	
P	pressure	$N{\cdot}m^{-2}$
Pr	Prandtl number	
$\tilde{q}$	dimensionless heat transfer rate	
R	residual vector	
Ra	Rayleigh number, Eq. (11)	
T	temperature	K
T_h	hot wall temperature	K
T_c	cold wall temperature	K
u, v, w	velocity components	$m{\cdot}s^{-1}$
u	solutions vector	
V	cavity volume	m^3
V_f	fin volume	m^3
x, y, z	Cartesian coordinates	m
W	cavity width	m

Greek symbols

α	thermal diffusivity	$m^2{\cdot}s^{-1}$
β	coefficient of volumetric thermal expansion	K^{-1}
λ	fin aspect ratio	
μ	viscosity	$N{\cdot}s{\cdot}m^{-2}$
ν	kinematic viscosity	$m^2{\cdot}s^{-1}$
ρ	density	$kg{\cdot}m^{-3}$
ϕ	fin volume fraction	

Subscripts

fin	relative to the fin
fluid	relative to the fluid
h	hot
opt	optimal
c	cold

Superscript

$(\tilde{\ })$	dimensionless variables

when the fin is attached to the hot wall of the enclosure. Due to cost and weigh constraints, the total volume of the fin was fixed. Two degrees of freedom were varied in order to determine the ideal configuration of the fin: the fin horizontal length, and the fin aspect ratio. The numerical results cover the range $10^3 \leqslant Ra \leqslant 10^5$. We delineate the conditions for which optimization opportunities are present, i.e., the range where the fin geometry plays a significant role for maximizing the total heat transfer rate.

2. Mathematical modeling

Consider the three-dimensional cubic enclosure differentially heated shown in Fig. 1. The left and right vertical walls are kept at uniform temperatures equal to T_h and T_c respectively, where $T_h > T_c$. The top, bottom, front and rear walls are considered perfectly adiabatic. The temperature difference between the T_h and T_c walls triggers buoyancy driven flows inside the cavity. Nonetheless, $(T_h - T_c)$ is assumed small enough so that the Boussinesq approximation is valid.

In general, heat transfer and fluid flow are greatly modified (enhanced or reduced) by the presence of an obstacle in a cavity [8–12]. In this paper, the "obstacle" considered is an internal fin made of a high thermal conductivity material, and it serves the function of enhancing the heat transfer rate from the hot to the cold wall. The fin is attached to the center of the hot wall, and its dimensions are a, b and c, as shown in Fig. 1. The flow is assumed to be laminar, and the thermophysical properties are considered constant. The present analysis is based on the steady-state version of the conservative equations for a Newtonian fluid,

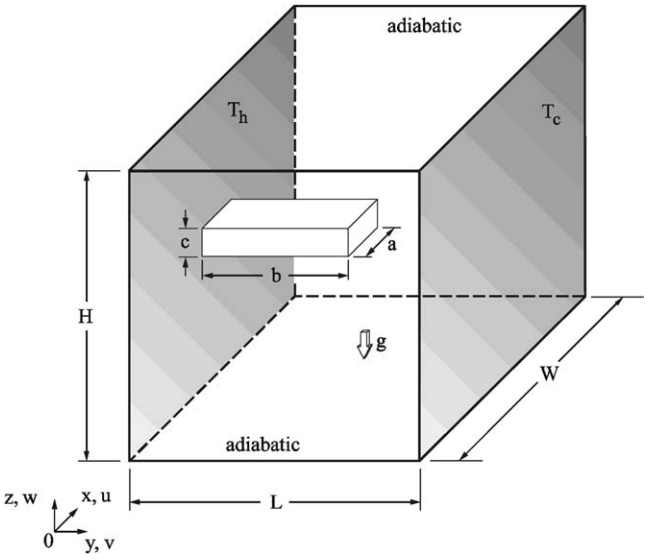

Fig. 1. The physical geometry and coordinate system.

$$\frac{\partial \tilde{u}}{\partial \tilde{x}} + \frac{\partial \tilde{v}}{\partial \tilde{y}} + \frac{\partial \tilde{w}}{\partial \tilde{z}} = 0 \tag{1}$$

$$\left(\frac{Ra}{Pr}\right)^{1/2}\left(\tilde{u}\frac{\partial \tilde{u}}{\partial \tilde{x}} + \tilde{v}\frac{\partial \tilde{u}}{\partial \tilde{y}} + \tilde{w}\frac{\partial \tilde{u}}{\partial \tilde{z}}\right) = -\frac{\partial \tilde{P}}{\partial \tilde{x}} + \nabla^2 \tilde{u} \tag{2}$$

$$\left(\frac{Ra}{Pr}\right)^{1/2}\left(\tilde{u}\frac{\partial\tilde{v}}{\partial\tilde{x}}+\tilde{v}\frac{\partial\tilde{v}}{\partial\tilde{y}}+\tilde{w}\frac{\partial\tilde{v}}{\partial\tilde{z}}\right)=-\frac{\partial\tilde{P}}{\partial\tilde{y}}+\nabla^2\tilde{v} \tag{3}$$

$$\left(\frac{Ra}{Pr}\right)^{1/2}\left(\tilde{u}\frac{\partial\tilde{w}}{\partial\tilde{x}}+\tilde{v}\frac{\partial\tilde{w}}{\partial\tilde{y}}+\tilde{w}\frac{\partial\tilde{w}}{\partial\tilde{z}}\right)=-\frac{\partial\tilde{P}}{\partial\tilde{z}}+\nabla^2\tilde{w}+\left(\frac{Ra}{Pr}\right)^{1/2}\tilde{T} \tag{4}$$

$$(Ra\,Pr)^{1/2}\left(\tilde{u}\frac{\partial\tilde{T}}{\partial\tilde{x}}+\tilde{v}\frac{\partial\tilde{T}}{\partial\tilde{y}}+\tilde{w}\frac{\partial\tilde{T}}{\partial\tilde{z}}\right)=\nabla^2\tilde{T} \tag{5}$$

where $\nabla^2=\partial^2/\partial\tilde{x}^2+\partial^2/\partial\tilde{y}^2+\partial^2/\partial\tilde{z}^2$, and the dimensionless variables are defined as

$$(\tilde{x},\tilde{y},\tilde{z},\tilde{L},\tilde{W},\tilde{a},\tilde{b},\tilde{c})=\frac{(x,y,z,L,W,a,b,c)}{H} \tag{6}$$

$$(\tilde{u},\tilde{v},\tilde{w})=\frac{(u,v,w)}{(\alpha/H)Ra^{1/2}Pr^{1/2}} \tag{7}$$

$$\tilde{T}=\frac{T-T_c}{T_h-T_c} \tag{8}$$

$$\tilde{P}=\frac{P}{(\mu\alpha/H^2)Ra^{1/2}Pr^{1/2}} \tag{9}$$

In Eqs. (7) and (9), Ra is the Rayleigh number ($Ra=g\beta\Delta T H^3/\nu\alpha$), and Pr the Prandtl number.

There is no flow in the fraction of the volume occupied by the fin (solid), and therefore only the energy equation (conduction) needs to be solved in that portion of the domain, $\nabla^2\tilde{T}=0$. The boundary conditions are: non-slip and no penetration for all surfaces inside the enclosure, $\tilde{T}=1$ on the left vertical wall and $\tilde{T}=0$ on the right vertical wall, $\partial\tilde{T}/\partial n=0$ for the top, bottom, front and rear walls, where n is the respective normal vector. Because the fin is attached to the hot wall, the temperature at its base is the same as the one of the hot wall, $\tilde{T}=1$. The temperature profile in the volume occupied by the fin is solved simultaneously with Eqs. (1)–(5) for the fluid portion of the domain. Just like the other thermophysical properties, the fin conductivity k_{fin} is assumed constant. In most of the simulations, a typical value of 6500 has been specified for the fin-to-fluid thermal conductivity ratio $\tilde{k}=k_{fin}/k_{fluid}$. This value has been obtained by considering an aluminum fin in an air filled cavity, at approximately 300 K.

3. Computational details and code validation

The differential system composed of Eqs. (5)–(9) was solved in the cubical domain of volume $\tilde{H}\times\tilde{L}\times\tilde{W}=1$, which includes the volume occupied by the fin, by using a finite element code [13]. The numerical domain was discretized non-uniformly by using 27 cubical nodes. The explicit appearance of the pressure was eliminated based on a penalty function, with an error factor of 10^{-8}. By using the pressure penalty function, the pressure is replaced in the momentum equations by

$$\tilde{P}=-\tilde{\varepsilon}^{-1}\left(\frac{\partial\tilde{u}}{\partial\tilde{x}}+\frac{\partial\tilde{v}}{\partial\tilde{y}}+\frac{\partial\tilde{w}}{\partial\tilde{z}}\right) \tag{10}$$

where $\tilde{\varepsilon}=\varepsilon/\mu$, and the continuity equation is discarded. The nonlinear equations resulting from the Galerkin finite element method were solved by the modified Newton scheme. The selection of this solution method for the nonlinear equations stems from the fact that by applying the modified Newton scheme, we avoid the computational expenses associated with the solution of a large matrix at each iteration. The modified Newton scheme does not compute a new Jacobian at each iteration, instead it fixes the iteration operator. This scheme can be far more economical than the well-known Newton–Raphson method as the factorization of the Jacobian matrix is required only at the first iteration. However, the savings in computational time is gained at the expense of slower convergence. The upwind formulation, which has the effect of weighting the advection operators toward the upstream direction, was also used to control the inherent instabilities trigged at relatively high values of Rayleigh number (i.e., $Ra\geqslant 10^5$). The convergence criteria used was

$$\frac{\|\mathbf{u}^{(i)}-\mathbf{u}^{(i-1)}\|}{\|\mathbf{u}^{(i)}\|}\leqslant 0.001 \quad\text{and}\quad \frac{\|\mathbf{R}(\mathbf{u}^{(i)})\|}{\|\mathbf{R}(\mathbf{u}^{(0)})\|}\leqslant 0.001 \tag{11}$$

where $\mathbf{u}$ is the solution vector, i is the iteration index and $\mathbf{R}$ is the residual vector.

In the present study, the computational time required to achieve the stipulated convergence criteria varied between 2 and 12 hours for $Ra=10^3$ and $Ra=10^5$ respectively, on a Sun Blade 1000 (Ultra Spark III) Unix machine.

A grid refinement was performed for each value of the Rayleigh number. The grid tests showed that a uniformly spaced mesh could be used in x and z direction. However in y direction a non-uniform mesh was selected, with the smaller elements located close to the hot wall. For Rayleigh number 10^3 and 10^4, the mesh independence was achieved with 21 nodes per unit of dimensionless length for the three axes. For $Ra=10^5$, 31 nodes per unit of dimensionless length were used.

The accuracy of the grid and of the code was verified by comparing the results obtained for a finless cubic enclosure with the available literature [14–16]. The figure of merit selected was the overall heat transfer rate at the hot wall, which is equivalent to the averaged Nusselt number, and is defined as follows

$$\tilde{q}=\frac{q}{k_{fluid}H(T_h-T_c)}=\int_0^1\int_0^1\left.\frac{\partial\tilde{T}}{\partial\tilde{y}}\right|_{\tilde{y}=0}\mathrm{d}\tilde{x}\,\mathrm{d}\tilde{z} \tag{12}$$

Numerical tests show that the overall heat transfer rate $\tilde{q}$ in the finless enclosure, Eq. (12), presents an agreement within 5 percent when compared with the literature throughout the range $10^3<Ra<10^5$. This is an important verification that demonstrates the equivalence between

different numerical approaches: Fusegi et al. [14] applied finite difference technique, Ha and Jung [15] used finite volume, and we are using finite elements. The numerical results are also consistent with analytical expressions derived in Ref. [2], i.e., that $\tilde{q}$ scales as $Ra^{1/4}$, or more precisely $\tilde{q} = 0.364(L/W)Ra^{1/4}$.

4. Fin volume constraint and fin geometry

Our objective is to study how the shape of the fin influences the overall heat transfer rate from the hot to the cold wall. It is obvious that the presence of the fin (extended surface) increases the solid–fluid surface area. At the same time, however, it modifies significantly the fluid flow pattern since the fin also acts as an obstacle or a partition. Consequently, both aspects influence the total heat transfer rate defined in Eq. (12): the extension of the heat exchange area between the fluid and heated solid surfaces, and the modification of the flow pattern.

In the pursuit of the better configuration, we consider that the total fin volume is constrained. In other words, only a given amount of high conductivity material is available. Fixing the fin volume or mass is equivalent to fixing the fraction ϕ of the enclosure occupied by the fin,

$$\phi = \tilde{a}\tilde{b}\tilde{c} \tag{13}$$

Because of weight and cost limitations, the volume of the fin is much smaller than the volume of the enclosure, hence $\phi \ll 1$.

Thanks to fin volume constraint, Eq. (13), only two degrees of freedom (DOFs) are required to fully characterize the fin geometry. We choose $\tilde{b}$ and $\lambda = \tilde{c}/\tilde{a}$ as these two DOFs. The first one corresponds to the length of the fin. The other DOF, λ, represents the cross-sectional aspect ratio of the fin. When $\lambda = 1$, the fin has a square cross-section. The extremes $\lambda \ll 1$ and $\lambda \gg 1$ correspond respectively to a horizontally and vertically positioned fin.

With the constraint shown in Eq. (13), the exposed area of the fin, i.e., the surface in contact with the fluid, can be written as $A/H^2 = [2(1+\lambda)(\tilde{b}\phi/\lambda)^{1/2}] + \phi/\tilde{b}$. It is essentially an increasing function of the fin length $\tilde{b}$, and is larger when $\lambda \ll 1$ and $\lambda \gg 1$.

It is worth to point out that, when ϕ is large, the total heat transfer rate is maximum when the fin touches the cold wall, establishing a conduction 'thermal bridge'. This happens because there is no heat flux 'strangulation' throughout the fin. In such a configuration, the heat transfer through the fin scales as $k_{\text{fin}}(T_{\text{h}} - T_{\text{c}})ac/L$, i.e., in view of the constraint (13) and in terms of the dimensionless variables introduced above: $\tilde{q}_{\text{fin,conduction}} \sim \tilde{k}\phi$. In Section 3, we noted that the heat transfer rate in the finless cavity scales as $Ra^{1/4}$. In the limit of $\tilde{q}_{\text{fin,conduction}} \gg \tilde{q}_{\text{fluid,convection}}$, the best design is always the one where the fin touches the cold wall. In that case, most of the heat will be evacuated by conduction via this high conductivity path (i.e., the fin). The optimization of the fin geometry to maximize the heat transfer rate is crucial when natural convection plays a significant role in front of the 'thermal bridge' effect described above. Based on scale arguments, this suggests that, in view of the heat transfer rate, fin geometric optimization is 'meaningful' when

$$\frac{Ra^{1/4}}{\tilde{k}\phi} \geqslant 1 \tag{14}$$

For example, when $Ra = 10^5$ and $\tilde{k} = 6500$, one can calculate that the critical ϕ for the natural convection to play a significant role before the 'thermal conduction bridge' effect is of the order of 10^{-3}. If ϕ is larger than that value, the heat transfer rate is not significantly affected by the cross-sectional aspect ratio.

An additional remark has to be made in line with the previous discussion. In many previous studies on finned enclosures [12], the fin surface temperature was considered constant, and equal to the temperature of the wall to which it is attached. The constant temperature boundary condition is based on the assumption that the fin conductivity is very large ($\tilde{k} \to \infty$). It is clear, in view of the heat transfer rate maximization, that this idealization is flawed. If $\tilde{k}$ is infinite, then the best configuration is always the one where the fin touches both walls ($\tilde{b} = 1$). The heat transfer rate in that case is also infinite, no matter what the fin cross-sectional aspect ratio λ is. In summary, the whole issue of optimizing the fin geometry stems from the finiteness of $\tilde{k}$.

5. Numerical results: effect of the fin geometry on the heat transfer rate for $Ra^{1/4}/(\tilde{k}\phi) \ll 1$

In this section, the focus is on finned cavity with a small value of $Ra^{1/4}/(\tilde{k}\phi)$ that is, when the conduction thermal bridge effect takes place. The value of ϕ and $\tilde{k}$ are set equal to 0.1 and 6500 respectively. This ensures that even for large Rayleigh number (e.g., $Ra = 10^5$) the number $Ra^{1/4}/(\tilde{k}\phi)$ is still small.

For low Rayleigh number ($Ra = 10^3$), diffusion (conduction) is the dominant heat transfer mechanism in the cavity. In other words, buoyancy forces are not strong enough to trigger significant convection. A coarse one-dimensional analysis based on the concept of thermal resistance can be applied to obtain the scale for $\tilde{q}$. The finned cavity can be reduced to a system of three thermal resistances. The first resistance is due to heat conduction from the base to tip of the fin, $b/(k_{\text{fin}}ac)$. In series with the first resistance, there is a second one corresponding to conduction in the fluid layer between the tip of the fin and the cold wall, $(L-b)/(k_{\text{fluid}}ac)$. Finally, conduction from the hot wall surface not covered by the fin $(HW - ac)$ to the cold wall is accounted for with a third resistance, $L/[k_{\text{fluid}}(HW - ac)]$, in parallel with the two previous ones. Using the dimensionless parameters introduced above, the total heat transfer rate reads as:

$$\tilde{q} = 1 + \frac{\phi(\tilde{k}-1)}{\tilde{k} - \tilde{b}(\tilde{k}-1)} \tag{15}$$

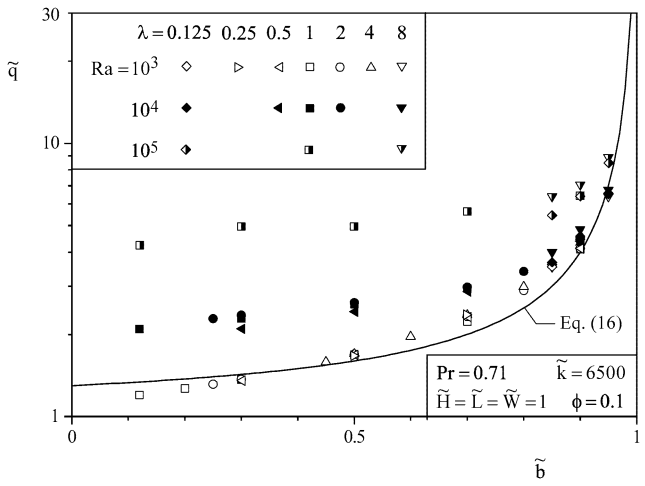

Fig. 2. The effect of the fin length and aspect ratio on the overall heat transfer rate when $Ra^{1/4}/(\tilde{k}\phi) < 1$.

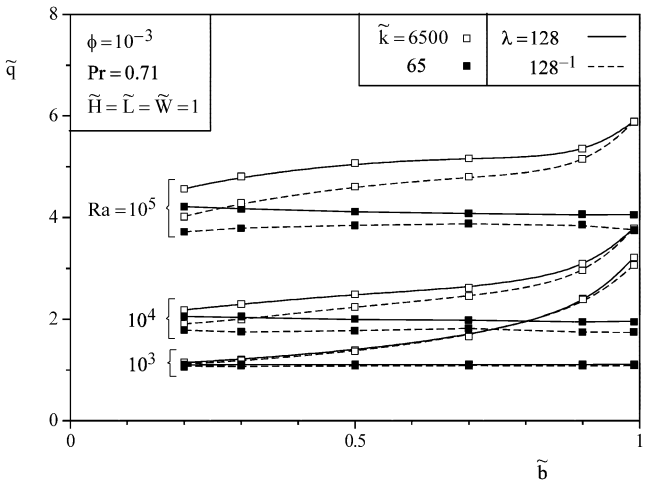

Fig. 3. The effect of the fin length and aspect ratio on the overall heat transfer rate when $Ra^{1/4}/(\tilde{k}\phi) \sim 1$, and $Ra^{1/4}/(\tilde{k}\phi) > 1$.

Because $\tilde{k} \gg 1$, Eq. (15) can be approximated by $\tilde{q} \sim 1 + \phi/(1-\tilde{b})$, provided that $\tilde{b} \neq 1$. Eq. (15) shows that $\tilde{q}$ is an increasing function of $\tilde{b}$, and that it is essentially independent of the fin cross-sectional aspect ratio, λ. This is also revealed in Fig. 2 (open symbols), where the numerical results have been reported for $Ra = 10^3$. It is clear from Fig. 2 and Eq. (15) that the maximum heat transfer rate for $Ra = 10^3$ is achieved when the fin tip touches the cold wall ($\tilde{b} = 1$), in which case Eq. (15) yields $\tilde{q} \sim 1 + \tilde{k}\phi$. The solid line presented in Fig. 2 is an adjusted version of Eq. (15), which shows that in the limit of $\tilde{k} \gg 1$, the numerical results for the heat transfer rate correlate within 11 percent with

$$\frac{(\tilde{q}-1)(1-\tilde{b})}{\phi} \sim 3 \tag{16}$$

As expected from Eq. (15), the number on the right-hand side of Eq. (16) is a number of order 1. When the Rayleigh number increases, natural convection gains in intensity. When Ra is of the order of 10^4 (solid symbols, Fig. 2), a modification of the dominant heat transfer occurs. One observes a transition from a conductive to a convective heat transfer regime, where the heat transfer rate for different values of λ are not as perfectly superimposed as when $Ra = 10^3$. Finally, Fig. 2 also presents the heat transfer rates for a cubic enclosure with a relatively large Rayleigh number ($Ra = 10^5$). In this case, buoyancy forces are sufficiently large to generate internal convective movements, and the shape of the fin (i.e., $\tilde{b}$ and λ) obviously influences the fluid flow pattern. We observe, that unlike the results for $Ra = 10^3$ and 10^4 shown in Fig. 2, $\tilde{q}$ now varies slightly with λ. In spite of that, the effect of λ on $\tilde{q}$ is still modest compared with the effect of $\tilde{b}$. Noting that, for a fixed $\tilde{b}$, the overall heat transfer rate for the configuration with $\lambda = 8$ is only slightly larger than $\tilde{q}$ for $\lambda = 0.125$. On the other hand, if the aspect ratio is held fixed, $\lambda = 1$ for example, $\tilde{q}$ increases by 30 percent from $\tilde{b} = 0.3$ to $\tilde{b} = 0.9$, which emphasizes the importance of the parameter $\tilde{b}$ on the enclosure performance. The low impact of λ on $\tilde{q}$ presented in Fig. 2 is in agreement with the transition proposed in Eq. (14): the largest value of the parameter $Ra^{1/4}/(\tilde{k}\phi)$ in Fig. 2 is 0.0273, hence $Ra^{1/4}/(\tilde{k}\phi) < 1$.

6. Numerical results: effect of the fin geometry on the heat transfer rate for $Ra^{1/4}/(\tilde{k}\phi) \sim 1$

Differently from all the numerical simulations reported up to this point, Fig. 3 presents the effect of the fin aspect ratio on the heat transfer rate for a fin that occupies only 10^{-3} of the volume of the enclosure and has a conductivity of $\tilde{k} = 6500$ (open symbols). At high values of the Rayleigh number ($Ra \sim 10^5$), the results in Fig. 3 show that the adequate selection of the fin aspect ratio (i.e., $\lambda \gg 1$) can increase $\tilde{q}$ by 15 percent when compared with $\lambda \ll 1$. Because of the limited amount of high conducting material, the temperature distribution in the fin is not uniform, especially when $\tilde{b}$ gets close to 1. Consequently, the heat transfer rate for $Ra \geqslant 10^4$ does not increase drastically with the fin length, $\tilde{b}$. Furthermore, as the Rayleigh number increases, the shape of the curves with constant aspect ratio changes. For low Rayleigh number, $Ra = 10^3$, the heat transfer rate is mainly a function of $\tilde{b}$, and the best configuration occurs when $\tilde{b} = 1$. For $Ra = 10^5$, the behavior of both constant λ curves suggests the existence of an optimal $\tilde{b} < 1$ for $Ra > 10^5$.

However, regardless of the Rayleigh number, the best performance is achieved when $\lambda \gg 1$, which corresponds to a vertically positioned fin that divides the cubic enclosure in two sub-cavities, each one of size $\tilde{H} \times \tilde{L} \times \tilde{W}/2$. The worst design in terms of the overall heat transfer rate is when $\lambda \ll 1$, i.e., when the fin is essentially a horizontal surface that creates two sub-cavities of dimensions $\tilde{H}/2 \times \tilde{L} \times \tilde{W}$.

The trend discussed above could have been anticipated from known finless cavity studies (Refs. [3–8]), by recognizing that in an enclosure fully filled by fluid, the x-dimension of the cavity (W) has a weak influence on the heat trans-

fer and fluid flow pattern as long as it is larger than δ_T, the boundary layer thickness. However, according to the available literature, the ratio (H/L) plays an important role on the thermal performance of differently heated cavities. Furthermore, studies of two-dimensional cavities in the y–z plane have demonstrated the existence of optimal aspect ratio $(H/L)_{opt}$, which enhances heat transfer and fluid flow. For example, according to Refs. [3] and [8], the optimal aspect ratio is $1.66 \leqslant (H/L)_{opt} \leqslant 1.37$ for $10^3 \leqslant Ra \leqslant 3 \times 10^4$. In any case, this optimal aspect ratio is a number slightly larger than 1.

In the present study, the condition $(H/L) \geqslant 1$ is satisfied for the sub-cavities $\tilde{H} \times \tilde{L} \times \tilde{W}/2$ in the limit $\lambda \gg 1$, and thus fluid flow patterns are not greatly modified compared with the finless cavity. However, in the limit $\lambda \ll 1$ the dimensions of the two sub-cavities are $\tilde{H}/2 \times \tilde{L} \times \tilde{W}$, i.e., that the aspect ratio is these sub-cavities is now $1/2$ which compares unfavorably with the aspect ratio of 1 in the other limit ($\lambda \gg 1$). The former is thus closer to the cavity optimal aspect ratio and leads to larger heat transfer rate and more intense fluid flow.

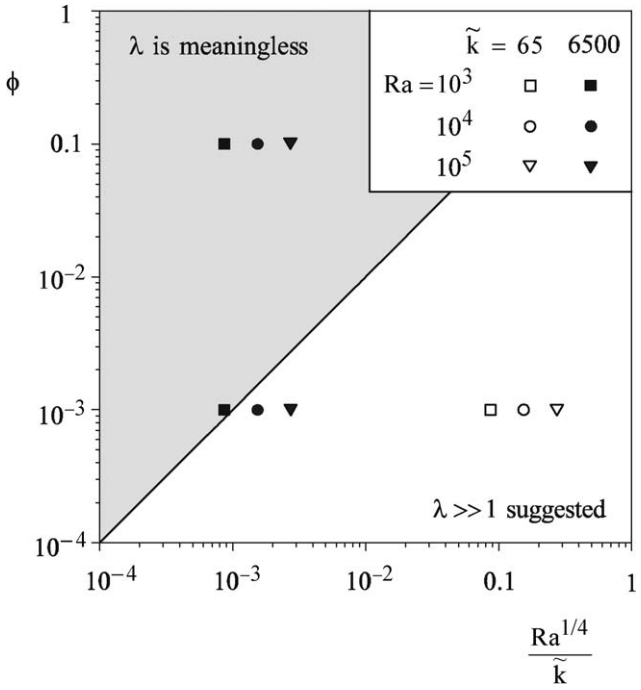

Fig. 4. The range in which the optimization opportunities in terms of cross-section aspect ratio lie in the (Ra–ϕ) plane, and the position of the numerical simulation in that plane.

7. Numerical results: effect of the fin geometry on the heat transfer rate for $Ra^{1/4}/(\tilde{k}\phi) \gg 1$

Next, we examine the optimization opportunities when $Ra^{1/4}/(\tilde{k}\phi)$ is large. To overcome the numerical difficulties related with large Rayleigh numbers or small ϕ-values, the value of $\tilde{k}$ has been decreased to 65 in order to obtain $Ra^{1/4}/(\tilde{k}\phi) \gg 1$. Note that even though $\tilde{k}$ is now much smaller than in the previous two sections, we still have $\tilde{k} \gg 1$, as dictated by the requirement to enhance the heat transfer rate. The results reported in Fig. 3 (i.e., solid symbols) show that the shape of the curves for fixed Ra and λ are different from the ones obtained in the previous sections ($\tilde{k} = 6500$). In the present case, the heat transfer rate is almost unaffected by $\tilde{b}$. Note that the heat transfer rate with $\lambda \gg 1$ (vertically positioned fin) is always the largest, no matter what Rayleigh number is considered. This is explained by the optimal shape of the sub-cavities, Section 6. The best geometry, however, is not necessarily achieved when $\tilde{b} = 1$, which is different from the previous cases.

8. Conclusions

The numerical results presented in this paper confirm the importance of the fin geometry in particular when the condition described by Eq. (14) is met. Fig. 4 shows the comparison between the theoretical transition determined in Eq. (14), and the numerical results. The symbols show where the numerical simulations presented previously in Figs. 2 and 3 lie in the Ra–ϕ plane. The gray shadow represents the region discussed in Section 5 (i.e., $\phi > Ra^{1/4}/\tilde{k}$). In this limit, the amount of high conductivity material is large and the optimization of the fin geometry is not essential, especially for low values of Ra. In the lower region, the open symbols suggest that conduction and convection heat transfer are at least of the same order of magnitude and the aspect ratio of the fin is an important parameter on the overall performance of the enclosure ($Ra^{1/4}/(\phi\tilde{k}) > 1$, Section 7). For the transition region (Section 6), the overall heat transfer rate delivered by the hot wall, $\tilde{q}$, increases with the fin horizontal length, $\tilde{b}$, even though the fin volume fraction is small ($\phi > 10^{-3}$), regardless of the fin aspect ratio. Also, values of $\lambda \gg 1$ are recommended close to the transition.

Additionally, for the limits discussed in Sections 5 and 6, the numerical results show that the best performance of the assisted cubic enclosure happens when the fin connects physically to the hot and cold walls, establishing a 'thermal bridge'. However, for fins of small volume fraction $\phi \sim 10^{-3}$ and low conductivity (Section 7), the overall heat transfer rate $\tilde{q}$ is essentially independent of the fin length.

Finally, we want to emphasize the idea that the modeling of a heat and fluid flow system should be guided by the system objectives and constraints. The objective of the fin is to enhance the overall heat transfer rate. Using a constant fin temperature approximation would lead to an "ill-posed" problem when the fin touches both walls, which is actually the optimal configuration in the limit $Ra^{1/4}/(\phi\tilde{k}) < 1$, but not necessarily in the other limit, $Ra^{1/4}/(\phi\tilde{k}) > 1$. It is thus necessary to solve the temperature equation within the fin in the quest for optimally finned cavity.

Acknowledgements

The authors acknowledge with gratitude the comments and support received on this article from Prof. Adrian Bejan (Duke University, Durham NC). A.K. da Silva also acknowledges the Brazilian Research Council – CNPq for the award of the Doctoral scholarship n^{o} 200021/01-0.

References

[1] H. Bénard, Les tourbillons cellulaires dans une nappe liquide, Rev. Gen. Sci. Pure Appl. 11 (1900) 1261–1271, 1309–1328.
[2] G.K. Batchelor, Heat transfer by free convection across a closed cavity between vertical boundaries at different temperatures, Q. Appl. Math. 12 (1954) 209–233.
[3] A. Bejan, A synthesis of analytical results for natural convection heat transfer across rectangular enclosures, Internat. J. Heat Mass Transfer 23 (1980) 723–726.
[4] A.T. Prata, T.A. Myrum, E.M. Sparrow, Numerical solution for natural convection in a complex enclosed space containing either air–liquid or liquid–liquid layers, Numerical Heat Transfer 10 (1986) 19–43.
[5] M.M. Ganzarolli, L.F. Milanez, Natural convection in rectangular enclosures heated from below and symmetrically cooled from the sides, Internat. J. Heat Mass Transfer 38 (1995) 1063–1073.
[6] A. Bejan, Convection Heat Transfer, second ed., Wiley, New York, 1995, Chapter 5.
[7] D.W. Pepper, K.G.T. Hollands, Summary of benchmark numerical studies for 3-D natural convection in an air-filled enclosure, Numer. Heat Transfer A 42 (2002) 1–11.
[8] R.L. Frederick, On the aspect ratio for which the heat transfer in differentially heated cavities is maximum, Internat. Comm. Heat Transfer 26 (1999) 549–558.
[9] A.K. da Silva, S. Lorente, A. Bejan, Optimal distribution of discrete heat sources on a wall with natural convection, Internat. J. Heat Mass Transfer 47 (2004) 203–214.
[10] G.N. Facas, Natural convection in a cavity with fins attached to both vertical walls, J. Thermophys. Heat Transfer 7 (1993) 555–560.
[11] E.K. Lakhal, M. Hasnaoui, E. Bilgen, P. Vasseur, Natural convection in inclined rectangular enclosures with perfectly conducting fins attached on the heated wall, J. Heat Mass Transfer 32 (1997) 365–373.
[12] Y. Yamaguchi, Y. Asako, Effect of partition wall on natural convection heat transfer in a vertical air layer, J. Heat Transfer 123 (2001) 441–449.
[13] FIDAP Manual, Fluid Dynamics International, Inc., 1998.
[14] T. Fusegi, J.M. Hyun, K. Kuwahara, B. Farouk, A numerical study of three-dimensional natural convection in a differentially heated cubical enclosure, Internat. J. Heat Mass Transfer 34 (1991) 1543–1557.
[15] M.Y. Ha, M.J. Jung, A numerical study on three-dimensional conjugate hat transfer of natural convection and conduction in a differentially heated cubic enclosure with a heat-generating cubic conduction body, Internat. J. Heat Mass Transfer 43 (2000) 4229–4248.
[16] S. Wakitani, Numerical study of three-dimensional oscillatory natural convection at low Prandtl number in a rectangular enclosure, J. Heat Transfer 123 (2001) 77–83.